Contemporary Engineering Sciences, Vol. 7, 2014, no. 6, 231 - 261
HIKARI Ltd, www.m-hikari.com
http://dx.doi.org/10.12988/ces.2014.3737

Constant False Alarm Rate Detection in Pareto Distributed Clutter: Further Results and Optimality Issues

Graham V. Weinberg

National Security and Intelligence Division
Defence Science and Technology Organisation
P. O. Box 1500 Edinburgh, South Australia, 5111, Australia

Abstract

The Pareto distribution has been validated recently as a model for X-band high resolution maritime surveillance radar clutter returns. As such, coherent and incoherent detection schemes have begun to appear in the literature. Consequently, constant false alarm rate (CFAR) detectors have also been explored in recent work. This paper introduces some new detectors, designed to manage issues associated with interfering targets and clutter changes in the CFAR training cells. Additionally, the existence of an optimal CFAR is examined, to see whether such a detector can exist as in the Gaussian intensity case.

Keywords: Constant false alarm rate radar, Incoherent detection, Pareto clutter, Gaussian targets, Detector performance, Interference, Clutter transitions

1 Background and Motivation

There has been an evolution in the development of clutter models for maritime surveillance radars operating at X-band, which is largely attributable to systematic improvement in radar resolution [1]. Earlier low resolution radar clutter returns were well modelled by Gaussian distributions [2]. As radar resolution improved, there has been an evolution in amplitude clutter models,

ranging from Lognormal, Weibull, K- and KK-Distributions [3-7]. Maritime radar clutter at X-band, and at high resolution, is characterised by very spiky statistics, and so long-tailed distributions became an obvious choice for the next generation of statistical clutter models.

As an example, Figure 1 shows two plots of actual spiky intensity maritime surveillance radar clutter returns. The left subplot is for the case of horizontal polarisation, while the right is for vertical polarisation. These have been obtained from the Defence Science and Technology Organisation (DSTO)'s high resolution X-band clutter data sets, which will be described in subsequent sections. What is important to note in Figure 1 is the appearance of false targets, which is attributable to the radar resolution and the fact that maritime sea clutter is very spiky at X-band.

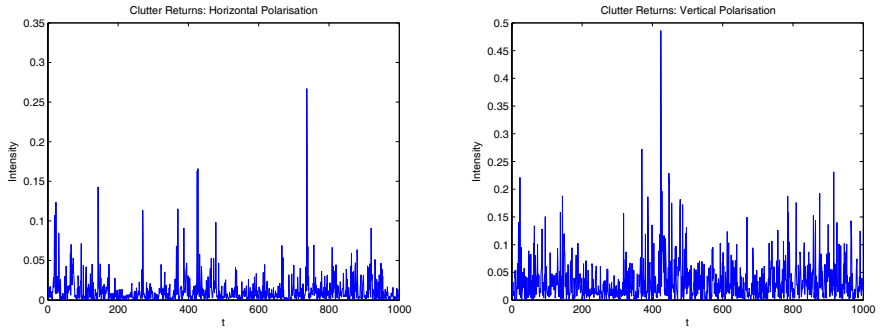

Figure 1: A time series of 1000 pure real intensity clutter returns, illlustrating the challenge in target detection in spiky sea clutter.

Figure 2 examines the correlations of the data plotted in Figure 1. Shown are plots of the associated autocovariance functions for the two sets of data. It is clear that there is significant correlations in the data, which is of a periodic nature. However, the strength of the correlations appears to be small.

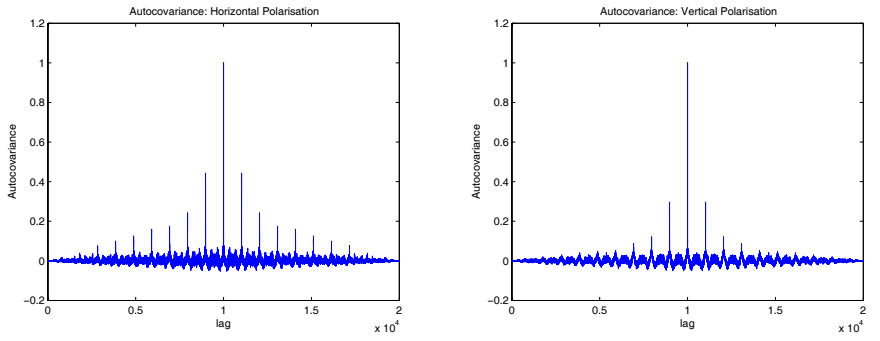

Figure 2: Autocovariance functions for the data in Figure 1, showing the dependency between sample observations.

The Pareto model first appeared in radar analysis in [8], in the context of modelling clutter as a compound Gaussian distribution with inverse Gamma texture. The Pareto distribution arises as the model's univariate intensity distribution [9]. This distribution is characterised by a very long tail. Validation of the Pareto model for low grazing angle maritime X-band clutter was reported in [10], and then further confirmed to fit the high grazing angle case in [11].

Coherent detection schemes, based upon a Pareto intensity model, have been analysed in several recent papers [9, 12-15]. From the incoherent perspective, [16] analyses classical integrators. Constant false alarm rate (CFAR) control is explored in [17], where a relationship between the Exponential and Pareto distributions is exploited to generate CFAR detectors. Included in this work is an investigation of the performance of three CFAR detectors, both in homogeneous and heterogeneous clutter environments. One of the interesting observations in this study was the apparent lack of optimal CFAR, in the sense that each of the three detectors could surpass the others performance, in different numerical experiments. The target model used was a Swerling 1 Gaussian model. Such a target model, when used in the context of CFAR detection in Gaussian clutter (with Exponential intensity returns), is known to result in the existence of an optimal CFAR detector [19]. It is hence of interest to investigate whether there is an optimal CFAR detector for the Pareto case, with a corresponding relevant target model.

The Pareto intensity distribution [19, 20], with shape parameter $\alpha > 0$ and scale parameter $\beta > 0$ has density

$$g_X(t) = \frac{\alpha\beta^\alpha}{t^{\alpha+1}}, \tag{1}$$

for $t \geq \beta$, and is zero otherwise. We write $X \stackrel{d}{=} Pa(\alpha, \beta)$ to signify that the random variable X has this distribution. Its cumulative distribution function is given by

$$G_X(t) = \mathbb{P}(X \leq t) = 1 - \left(\frac{\beta}{t}\right)^\alpha, \tag{2}$$

for $t \geq \beta$, where $\mathbb{P}$ denotes probability.

To illustrate the Pareto clutter fit to DSTO's data, Figure 3 performs a quantile-quantile (QQ) plot for the full set of data associated with Figure 1. Pareto clutter parameters have been estimated in Matlab to generate a corresponding comparison distribution. For the horizontally polarised case, these are $\alpha = 4.7241$ and $\beta = 0.0446$. The vertically polarised case has $\alpha = 11.3930$ and $\beta = 0.3440$. Smaller shape parameters indicate spikier returns [11]. The subplots in Figure 3 plot the sample quantiles against those obtained with the corresponding theoretical distribution. These results show the difficulty in

getting an accurate fit for the horizontally polarised case. There is a better fit in the vertical polarised scenario. These results are examined in [11], and it was found the Pareto fit matched those for the K- and KK-Distributions. Given the relative simplicity of the Pareto model, this further justifies the development of radar detectors based upon this clutter model assumption.

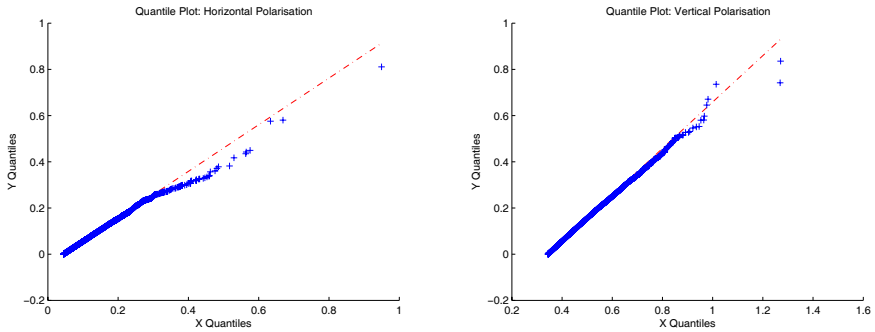

Figure 3: Quantile comparison plots, for the data of which the clutter in Figure 1 is a subset.

This paper extends the detectors introduced in [17], with the motivation being the development of improved CFAR detectors for target detection when the clutter training cells contain interfering targets. Additionally, it is imperative that such a detector can perform well in the presence of clutter transitions. This is measured by the ability of a CFAR to preserve the false alarm probability, when the CFAR clutter cells are gradually affected by higher powered returns.

In addition to this, the existence of an optimal CFAR detector in homogeneous Pareto clutter is explored. Here, optimality is in the sense of a uniformly most powerful (UMP) test [20] generating a decision rule which has maximum probability of detection, for a given false alarm probability.

This paper is organised as follows. Section 2 fomulates the CFAR problem, while Sections 3 - 5 introduce the new detectors. Section 6 analyses detector performance in homogeneous clutter. Sections 7 and 8 analyse detector performance in the heterogeneous clutter scenario. Finally, Sections 9 and 10 examine the question of the existence on an optimal CFAR detector for targets in homogeneous Pareto distributed clutter.

A useful reference on CFAR detection is [22], while [20] is a good reference on statistical hypothesis tests. Probability distribution properties can be sourced from [19, 20].

2 Formulation of the CFAR Problem

The central idea behind CFAR detection is that we have a series of N independent and identically distributed clutter intensity statistics $X_1, X_2, \ldots, X_N$, from which an "average" level of clutter is produced through the application of some function f. These clutter statistics are often referred to as the CFAR training or clutter range cells. When sampling from a real series of clutter returns, obtained from an operational radar, these will be subsampled from the data stream so that they are approximately uncorrelated returns. The measurement of clutter level obtained from the range cells is then normalised using a threshold multiplier τ, such that the probability of false alarm depends only on this threshold multiplier, and not on the clutter statistics. Due to sensitivity between the detection threshold/probability of false alarm and clutter parameters, the hope in the CFAR approach is that this sensitivity can be eliminated by using an *ad hoc* suboptimal detector [22, 23]. The tradeoff in not using a decision rule based upon the Neyman-Pearson Lemma [20] is a likely reduction in detection performance [23].

A cell under test (CUT) is then assessed to see whether a target is present or not. It is assumed that this is independent of the clutter statistic cells, which is achieved by allowing for a sufficient number of guard cells in the range profile under examination [22]. As a statistical hypothesis test, if we suppose H_0 is the hypothesis that the CUT is pure clutter, and H_1 is the hypothesis that the CUT is a mixture of target return and clutter, then the decision rule takes the form

$$Z \underset{H_0}{\overset{H_1}{\gtrless}} \tau f(X_1, X_2, \ldots, X_N)/N, \tag{3}$$

where Z is the statistic of the CUT, and the notation $A \underset{H_0}{\overset{H_1}{\gtrless}} B$ means that we reject the null hypothesis if any only if the statistic $A > B$.

It has been shown that for the case of Gaussian intensity returns, and with a Swerling 1 target model, the cell averaging CFAR, where f is a sum, is the optimal CFAR [19].

In recent years the effect of transformations on UMP tests has been explored [24], showing such properties can be preserved under some transformations of decision rules. Given the duality between Exponential and Pareto random variables, this created an interest in further exploring this phenomenon in the Pareto case.

To see this duality, as explained in [17], if $X \overset{d}{=} Pa(\alpha, \beta)$, and Y is an Exponential random variable with parameter α, (written $Y \overset{d}{=} Exp(\alpha)$) then these two distributions are related by

$$X = \beta e^Y, \tag{4}$$

where Y has density given by $g_Y(t) = \alpha e^{-\alpha t}$, for $t \geq 0$, and is zero otherwise.

This was the key in [17] to transforming simple Gaussian intensity CFAR processes to the Pareto case. The basic approach is to start with a CFAR detector for the Gaussian intensity case, and then to transform the expression for the detector using the inverse of (4), so that it is in terms of Pareto clutter statistics. This results in a detector operating on Pareto clutter, whose probability of false alarm and threshold multiplier relationship will be identical to that for the pre-transformed Gaussian counterpart.

An inevitability of using the transformation (4) is that the detectors require explicit knowledge of the Pareto scale parameter. Hence it will be assumed that β is explicitly known. As argued in [17], since this parameter is not critical to determining the distribution's shape, this assumption is reasonable. Further, given the development of improved Pareto parameter estimation prodedures in [18], β can be estimated very accurately for small sample sizes. Hence in all the analysis to follow, β is assumed known while α is assumed to be unknown but fixed. Hence, strictly speaking, the CFAR processes developed are CFAR with respect to α.

Using (4), three simple CFAR processes were constructed in [17], which were extensions of the Gaussian intensity cell-averaging CFAR, as well as the minimum and maximum CFAR-based detectors. As an example, a geometric mean variant, also known as a product detector in [17], is defined by

$$Z \underset{H_0}{\overset{H_1}{\gtrless}} \beta^{1-N\tau} \prod_{j=1}^{N} X_j^{\tau}, \tag{5}$$

which is shown to have its probability of false alarm related to τ by $\mathbf{Pfa} = (1+\tau)^{-N}$. The latter expression can be recognised at the probability of false alarm and threshold multiplier relationship for the cell-averaging CFAR detector for the Gaussian intensity case [23]. Additionally, the transformation approach of [17] results in a CFAR detector significantly different in form from the traditional CFARs analysed in the literature.

Using the relationship (4), a series of new detectors are now introduced, based upon transformations of Gaussian intensity CFARs. The importance of extending the detectors in [17] lies in the need to develop CFAR processes that can manage multiple targets that may appear in the CFAR range cells. Additionally, preservation of the false alarm probability is required in the case where the clutter power may fluctuate.

3 Order-Statistic CFAR

As an extension of the minimum and maximum-based CFARs in [17], a general order statistic CFAR (OS-CFAR) can be defined. If we let $X_{(k)}$ be the k^{th} OS

of the clutter returns, then

$$Z \underset{H_0}{\overset{H_1}{\gtrless}} \beta^{1-\tau} X_{(k)}^{\tau} \tag{6}$$

can be proposed as a detector. It is now shown that the probability of false alarm and threshold multiplier do not depend on the clutter parameters, and hence the clutter power. To facilitate the calculation, it is shown in [18] that the k^{th} OS for a series of independent and identically distributed Pareto random variables can be written

$$X_{(k)} = \beta W_k^{-1/\alpha}, \tag{7}$$

where W_k is a Beta distribution with parameters $N-k+1$ and k [20]. By applying this, together with the fact that under H_0, the cell under test statistic can be written $Z = \beta e^Q$, where Q has an Exponential distribution with parameter α (see (4)),

$$\begin{aligned} \mathbf{Pfa} &= \mathbb{P}(Z > \beta^{1-\tau} X_{(k)}^{\tau}) = \mathbb{P}(e^Q > {W_k}^{-\tau/\alpha}) \\ &= \int_0^1 f_{W_k}(t) \mathbb{P}(Q > \log(t^{-\tau/\alpha})) dt \\ &= \int_0^1 t^{\tau} f_{W_k}(t) dt, \end{aligned} \tag{8}$$

where f_{W_k} is the density of W_k, and statistical conditioning has been used. By applying the density of the Beta distribution to (8), and then by an application of the Beta function and its relationship to the Gamma function, it is not difficult to show that (8) reduces to

$$\mathbf{Pfa} = \frac{N!}{(N-k)!} \frac{\Gamma(N-k+\tau+1)}{\Gamma(N+\tau+1)}, \tag{9}$$

where $\Gamma(\cdot)$ is the Gamma function [20]. Hence detector (6) is CFAR with respect to α. In order to set the threshold multiplier τ, for a given probability of false alarm, one can invert the expression (9) numerically.

4 Smallest-Of and Greatest-Of CFAR

Next, smallest-of (SO) and greatest-of (GO) CFARs are introduced. By transforming the Gaussian intensity equivalent, it can be shown the detector takes the form

$$Z \underset{H_0}{\overset{H_1}{\gtrless}} \beta^{1-M\tau} \left(\underset{max}{min} \left(\prod_{j=1}^{M} X_j, \prod_{j=M+1}^{N} X_j \right) \right)^{\tau}, \tag{10}$$

where *min* is used for SO-CFAR and *max* is for GO-CFAR, and for simplicity we have assumed that N is even, and $M = N/2$. The false alarm probabilities are given by

$$\mathbf{Pfa}_{\mathrm{GO}} = 2(1+\tau)^{-M} - \mathbf{Pfa}_{\mathrm{SO}}, \tag{11}$$

where

$$\mathbf{Pfa}_{\mathrm{SO}} = 2\sum_{j=0}^{M-1} \left(\begin{array}{c} M+j-1 \\ j \end{array} \right) (2+\tau)^{-(M+j)}. \tag{12}$$

Hence it follows that (10) is CFAR with respect to α. The GO-CFAR censors the lower half of the clutter statistics, while the SO-CFAR censors the upper half. The subscripts in expressions (11) and (12) indicates the corresponding CFAR scheme, and these results have been obtained from [25].

The proof of the expressions for probability of false alarm is a relatively straightforward application of (4) to the Gaussian CFAR equivalent in [25]. It is illustrated for the case of the GO-CFAR only. Under H_0, we can write $Z = \beta e^Q$, where $Q \stackrel{d}{=} Exp(\alpha)$. Additionally, each $X_i = \beta e^{Y_i}$, where $Y_i \stackrel{d}{=} Exp(\alpha)$. Using the fact that the maximum and logarithm function are exchangeable,

$$\begin{aligned} \mathbf{Pfa} &= \mathbb{P}\left(\log(Z\beta^{M\tau-1}) > \tau \max\left(\log\prod_{j=1}^{M} X_j, \log\prod_{j=M+1}^{N} X_j \right) \right) \\ &= \mathbb{P}\left(Q + M\tau\log(\beta) > \tau \max\left(\sum_{j=1}^{M} \log(\beta) + Y_j, \sum_{j=M+1}^{N} \log(\beta) + Y_j \right) \right) \\ &= \mathbb{P}\left(Q > \max\left(\sum_{j=1}^{M} Y_j, \sum_{j=M+1}^{N} Y_j \right) \right). \end{aligned} \tag{13}$$

Consequently, it follows that the probability of false alarm (13) is that for the Gaussian intensity GO-CFAR, and so an application of the results in [25] completes the proof. Extension of this to the SO-CFAR equivalent is straightforward.

Again, in practical implementation, the threshold multiplier τ is obtained from (11) and (12) via numerical inversion.

5 Trimmed-Mean CFAR

A trimmed mean (TM) CFAR can also be constructed, which is based upon censoring applied to ordered clutter statistics in (5). In particular, the TM-

CFAR is

$$Z \underset{H_0}{\overset{H_1}{\gtrless}} \beta^{1-(N-T_1-T_2)\tau} \left(\prod_{j=T_1+1}^{N-T_2} X_{(j)} \right)^{\tau}, \tag{14}$$

where T_1 statistics are trimmed from the lower OS, while T_2 are trimmed from the top. By applying the fact that if $Z_{(k)}$ is the k^{th} OS for a series of Exponentially distributed random variables with parameter α, then the k^{th} OS for a series of Pareto random variables is given by $X_{(k)} = \beta e^{Z_{(k)}}$, it can be shown that the TM-CFAR has probability of false alarm given by

$$\mathbf{Pfa} = \prod_{j=1}^{N-T_1-T_2} M_{\nu_j}(\tau), \tag{15}$$

where the function

$$\begin{aligned} M_{\nu_1}(\tau) &= \frac{N!}{T_1!(N-T_1-1)!(N-T_1-T_2)} \times \\ &\quad \sum_{j=0}^{T_1} \frac{\binom{T_1}{j}(-1)^{T_1-j}}{\left(\frac{N-j}{N-T_1-T_2}\right)+\tau}, \end{aligned} \tag{16}$$

and for $2 \leq j \leq N - T_1 - T_2$

$$\begin{aligned} M_{\nu_j}(\tau) &= \frac{a_j}{a_j+\tau} \\ \text{where } a_j &= (N-T_1-j+1)/(N-T_1-T_2-j+1). \end{aligned} \tag{17}$$

Hence detector (14) has the CFAR property with respect to α. Expression (15) can be found in [25], from the Gaussian intensity equivalent. The proof is omitted for brevity.

Observe that with the choice of $T_1 = T_2 = 0$, the detector (5) is recovered, while for the choice of $T_1 = k - 1$ and $T_2 = N - k$, the k^{th} OS-CFAR (6) is produced, for $1 \leq k \leq N$. From a theoretical perspective, a detector that censors T_1 lower and T_2 upper clutter statistics can be used to censor out an expected number of higher-powered interfering targets. It should also be able to tolerate clutter transitions to a certain point. As in the previous cases, τ is determined from (15) with numerical inversion.

6 Detector Performance in Homogeneous Clutter

6.1 Vertical Polarisation Examples

As an initial examination of detector performance, it is assumed that the clutter is homogeneous. Several examples of performance will be analysed,

with clutter simulated using parameters estimated from real data sets. Figure 4 shows CFAR detector performance for the three detectors introduced in [17] (denoted CFAR-Prod, CFAR-Min and CFAR-Max respectively). In addition, the OS, SO, GO and TM versions introduced in the previous sections are included. These are denoted CFAR-OS, CFAR-SO, CFAR-GO and CFAR-TM respectively. In all cases, performance is measured by plotting the probability of detection (Pd) as a function of the signal to clutter ratio (SCR). Monte Carlo sampling with 10^6 runs has been used for each detection probability estimate. The target model used is a Swerling 1 Gaussian model, as in [17].

The first example considered corresponds to the case where $N = 8$ and the probability of false alarm is 10^{-2}. The motivation for choosing such a large false alarm probability was so that the minimum CFAR would not saturate. In this example, the clutter has parameters based upon Ingara data set run 34690, at an azimuth angle of 225°, with vertical polarisation. Details on the Ingara radar and clutter analysis can be found in [26] and [27] . The Pareto model fit to the Ingara clutter is described in [11]. The clutter parameters were estimated to be $\alpha = 15.8983$ and $\beta = 0.1812$. The OS-CFAR used the 9^{th} observation, while the TM-CFAR removed the largest two observations. The SO- and GO-CFARs are based upon censoring exactly half the observations. Figure 4 shows that many of the detectors are matching almost exactly the performance of the ideal CFAR (denoted CFAR-Ideal) introduced in [17]. Figure 5 shows a magnification of Figure 4, which demonstrates the product CFAR (5) is dominant. The minimum CFAR ((6) with $k = 1$) has the worst performance.

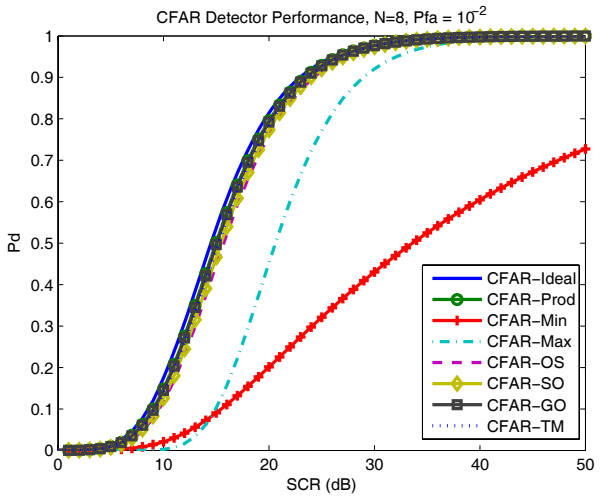

Figure 4: Examples of detector performance in vertically polarised clutter. Shown are the detectors in [17], as well as the three new detectors introduced, together with an ideal CFAR.

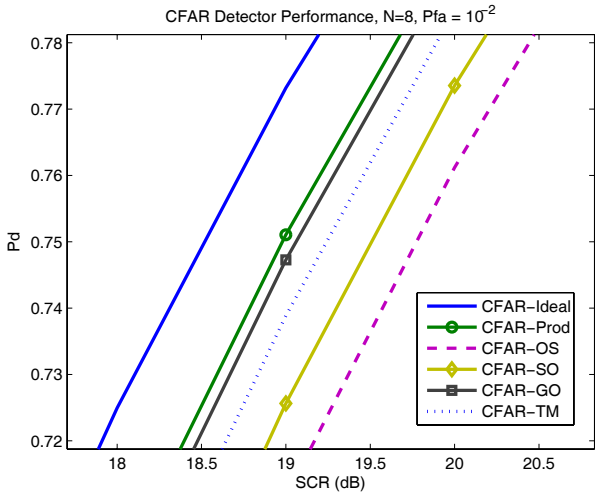

Figure 5: A magnification of the detectors in Figure 1. Here we observe that the product-based detector (5) has the best performance.

A second example of detector performance with vertical polarisation is provided in Figure 6. This has been based upon the DSTO Ingara data set run 34683, with azimuth angle of 225°. In this case, the Pareto fitted parameters are $\alpha = 11.3930$ and $\beta = 0.3440$. This is the data set used to produce Figure 1 (right subplot). Here we have selected $N = 16$ and the false alarm probability is 10^{-6}. In this case, $T_1 = 3$ and $T_2 = 2$. The OS-CFAR uses $k = 8$. In this example the maximum-CFAR has the best performance, followed by the product CFAR. The TM- and GO-CFAR closely match the product CFAR. The OS-CFAR has poor performance, while the minimum saturates.

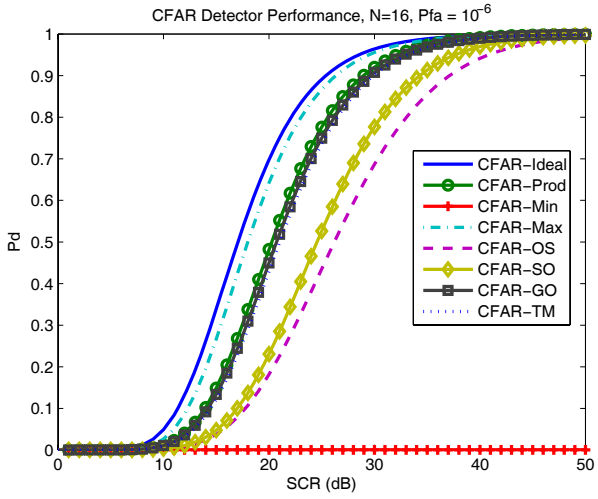

Figure 6: Detector performance in homogeneous vertically polarised clutter.

6.2 Horizontal Polarisation Examples

Next an example of performance in horizontally polarised clutter is provided. In this case, the clutter parameter estimates have been based upon Ingara data set run 34685, at an azimuth angle of 225°. The Pareto clutter parameters have been estimated to be $\alpha = 4.4525$ and $\beta = 0.0147$. The number of CFAR training cells is $N = 18$ and the false alarm probability is 10^{-6}. Figure 7 shows the detector performance. Due to the spikier clutter returns, the detectors experience difficulties in finding a target with SCR < 10 dB. This is also attributable to the application of suboptimal detectors. Figure 7 shows that the maximum-CFAR of [17] has the best performance, followed by the product CFAR. The minimum CFAR completely saturates in this example. Here the OS-CFAR uses the 4^{th} OS, while the TM-CFAR again censors the largest two observations. The SO-and GO-CFAR are based upon products of 9 clutter statistics. As a second example of performance in very spiky clutter, Figure 8

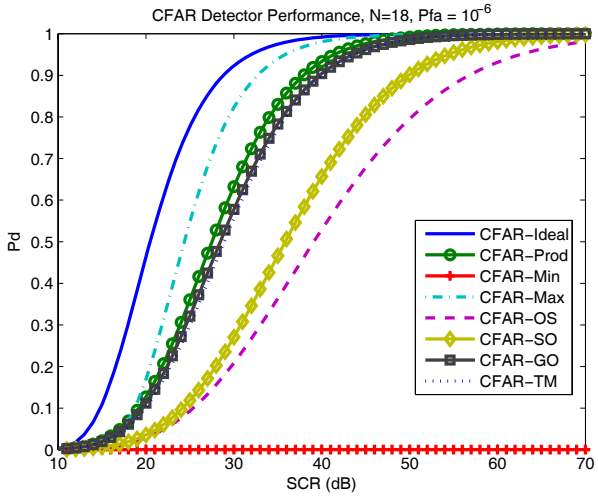

Figure 7: Detector performance in horizontally polarised clutter, using the Ingara data clutter parameter estimates.

shows detector performance with Pareto clutter whose parameters are sourced from the McMaster University's IPIX radar. Details of this radar can be found in [28], which includes analysis of the data obtained from it. Additionally, [8] examines clutter modelling of the data obtained from this radar. For the example considered here, the polarisation is horizontal, and the fitted clutter parameters are $\alpha = 1.5582$ and $\beta = 4.3286 \times 10^{-4}$. Figure 8 shows the detector performance, when $N = 6$ and the false alarm probability is 10^{-4}. The OS-CFAR uses the 3^{rd} OS, while the TM censors the two largest observations, as before. Here the maximum CFAR has near optimal performance, while the other detectors experience great difficulty because of the very spiky returns.

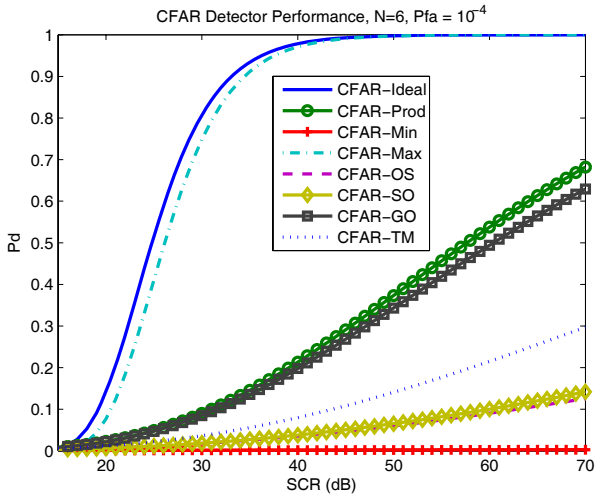

Figure 8: Detector performance, again with horizontally polarised clutter, but with Pareto parameter estimates based upon the IPIX radar clutter.

Figures 4 - 8 highlight the observation in [17] that there is no dominant CFAR, with respect to the Swerling 1 target model. However, when the clutter is more Gaussian, as occurs in the vertically polarised clutter case, it is expected that (5) should be near optimal with a Swerling 1 target model. The observations in [17] found that the maximum CFAR had near optimal performance for a number of different cases. A good example of this can be found in Figure 9, which is again based upon horizontally polarised clutter. Here the Pareto parameters have been estimated from Ingara data set run 34683, at azimuth angle of 225°. The parameter estimates are $\alpha = 4.7241$ and $\beta = 0.0446$, which are estimated from the data plotted in Figure 1 (left subplot). For this example, $N = 16$ and the false alarm probability is 10^{-6}. Additionally the TM-CFAR uses $T_1 = 3$ and $T_2 = 2$, while the OS-CFAR uses $k = 4$. Here we see that the Max-CFAR matches very closely the performance of the ideal detector.

These examples show that the new CFARs do not provide much of a benefit in homogeneous clutter returns. However, it will be shown that the TM-CFAR can be very useful in the non-homogeneous clutter case.

7 Management of Interfering Targets

7.1 Detector Parameter Selection

Although the new CFARs did not provide any improvement on the detectors introduced in [17], their merit in application results from an analysis of detector performance when the CFAR training cells are subjected to inter-

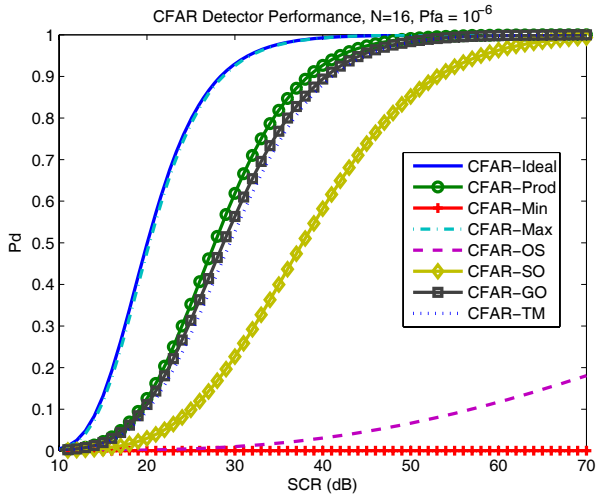

Figure 9: Detector performance in homogeneous clutter, with horizontal polarisation, where the Maximum-CFAR matches the Ideal-CFAR detector very closely.

fering targets. Although the maximum-CFAR has excellent performance in homogeneous clutter, it will inevitably suffer with the addition of at least one significant range cell target. The product CFAR will also suffer the same performance issues. The SO-CFAR will invariably avoid this problem, but due to the fact it is based upon a subsample of the clutter range statistics, the smaller sample size will also reduce its performance. Additionally, as demonstrated in [17], this detector tends to saturate in practice. Clearly the GO-CFAR will suffer serious performance degragation in the presence of interference.

By contrast, the OS- and TM-CFAR have the potential to rectify these issues. In particular, the TM-CFAR can be designed to accommodate an expected number of interfering targets. It also has the capacity to filter out smaller interfering targets because it can censor both the lower and upper spectrum of excessive returns. Given these observations, only these two CFARs will be analysed in the work to follow.

In order to select an appropriate k for the OS-CFAR, in view of [17], it is important that k is not too close to the expected number of interfering targets. Hence, for example, if one wanted to accommodate the possibility of 2 interfering targets, it would be necessary to select a $k < N - 1$. Given the tendency for the minimum-CFAR to saturate, it is hence important to select a $k > 1$. Hence a k can be selected such that $2 \leq k \leq N - 2$. A general approach could be to base the selection on the basis that if there are interfering targets, they should appear in the top 20% of statistics. Hence we can select $k = [0.8N]$, where $[x]$ is the greatest integer not exceeding x.

For the design of a TM-CFAR, we can select T_1 and T_2 by similar consid-

erations. One approach is to trim 10% of the statistics from the bottom, and 20% from the top end. Hence we can select $T_1 = [0.1N]$ and $T_2 = [0.2N]$. Censoring more statistics at the top end makes the detector more robust to stronger interfering targets.

These detector parameter selection methods introduce what will be termed an automatic censoring algorithm for the OS- and TM-CFARs.

7.2 Horizontal Polarisation Examples

For the sake of simplicity, attention is restricted to clutter generated from a Pareto distribution with parameters $\alpha = 4.7241$ and $\beta = 0.0446$, which have been discussed previously. Here we are interested in the analysis of the performance of the OS- and TM-CFARs, with detector parameter selection based upon the guidelines specified previously. For the purposes of exploration, three interfering targets have been used, and the effect of varying N and the probability of false alarm is examined.

In the first case the probability of false alarm is set to 10^{-5}, while $N = 10$. The OS- and TM-CFAR are subjected to up to three independent interfering targets in the training cells, each with a SCR of 2 dB. Figure 10 shows the performance of the detectors. The Figure shows the TM-CFAR has slightly better performance than the OS-CFAR when there is no interference. As the number of interfering targets in the range cells increase, both detectors experience loss. However the TM-CFAR tends to perform the best. The automatic censoring uses $T_1 = 1$, $T_2 = 2$ and $k = 8$. Hence the TM-CFAR effectively eliminates up to two strong interfering targets. The detection loss is also attributable to the reduction in the number of available clutter cells for processing.

Figure 11 shows the effect of increasing the number of clutter cells N to 16, while maintaining the probability of false alarm and SCR of the interfering targets. The censoring algorithm selects $T_1 = 2, T_2 = 3$ and $k = 13$. Here we see that the TM-CFAR eliminates all three interfering targets, and the overall detector performance has improved. The OS-CFAR trails the performance of the TM-CFAR.

Figure 12 shows the performance when N is increased to 32. For this scenario, the censoring algorithm has chosen $T_1 = 3, T_2 = 6$ and $k = 26$. Thus, the TM-CFAR can eliminate up to 6 strongly interfering targets. The Figure shows the same general results as noted before, except with a significant improvement in detection performance.

To complete our analysis, we consider the case where the probability of false alarm is decreased to 10^{-6}, while the three targets have SCR increased to 10 dB. Figure 13 shows detector performance when $N = 16$. The censoring algorithm has selected $T_1 = 2$, $T_2 = 3$ and $k = 13$. Hence the TM-CFAR eliminates the interfering targets. Increasing N to 32 results in improved

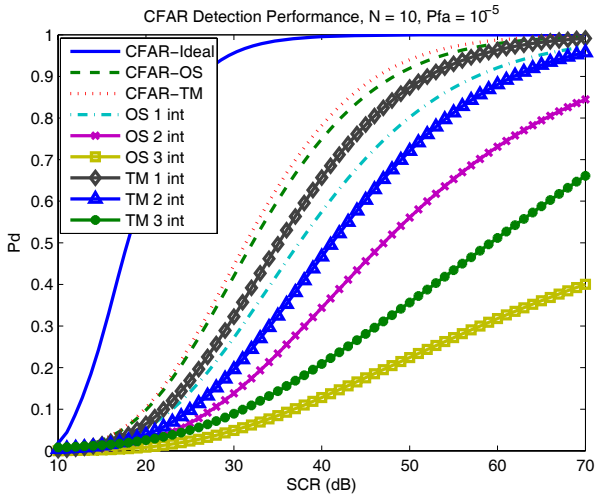

Figure 10: Detector performance in horizontally polarised clutter, when there are up to three interfering targets in the range cells. 'OS 1 int' refers to the OS-CFAR where there is one interfering target, 'TM 1 int' refers to the TM-CFAR where there is one interfering target, *et cetera*. The interfering targets each have a SCR of 2 dB.

detector performance, as illustrated in Figure 14. In this case, $T_1 = 3$, $T_2 = 6$ and $k = 26$.

7.3 Vertical Polarisation Examples

The main difference with detection in vertically polarised clutter with interfering targets is improvement in detector performance, as in the homogeneous clutter case. Examples considered for this polarisation are based upon the Pareto distribution with parameters $\alpha = 15.8983$ and $\beta = 0.1812$. In the first example, shown in Figure 15, $N = 16$ and the false alarm probability is 10^{-6}. Each interfering target has SCR of 10 dB. The censoring algorithm has selected $T_1 = 2$, $T_2 = 3$ and $k = 13$. Hence the TM-CFAR should be immune to the effects of up to three interfering targets. Here we see the TM-CFAR works very well, and experiences a detection loss with the reduction in the number of available clutter range cells. Increasing N improves its performance. The OS-CFAR always seems to be inferior to the TM-CFAR, as in previous cases considered.

For a final example, Figure 16 also uses $N = 16$, but with the false alarm rate has been decreased to 10^{-8}. Due to the lack of change in N, the censoring parameters remain the same. Again, the three interfering targets have SCR of 10 dB. The same phenomenon is repeated as illustrated in Figure 15.

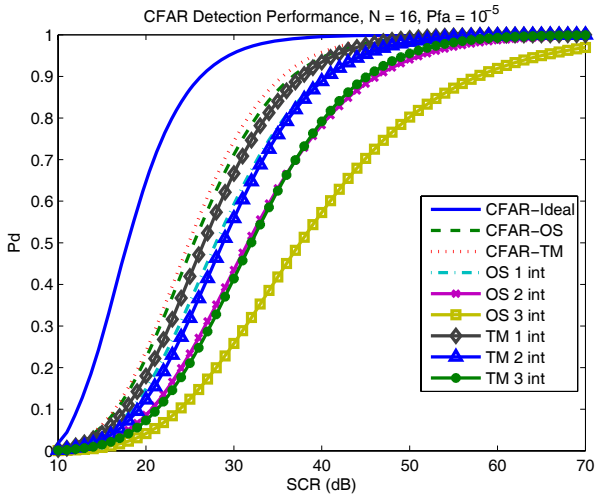

Figure 11: Detector performance with interfering targets, with same scenario as for Figure 10, except the number of clutter range cells is increased to 16. This increase results in improved performance in all cases.

7.4 Conclusions

The OS- and TM-CFARs were examined in the presence of up to three interfering targets in the clutter range cells. Adopting an automatic censoring algorithm resulted in the TM-CFAR managing interfering targets very well, and generally better than the OS-CFAR. When these results are compared to the detectors introduced in [17], their performance can be seen to be a major improvement in the management of interfering targets. If we want to manage a certain number of possible interfering targets, an appropriate censoring level can be determined, as illustrated. Increasing the number of clutter range cells will also improve detector performance when censoring is applied.

8 Performance during Clutter Transitions

The previous Section demonstrated that the TM-CFAR is robust with respect to interfering targets in the clutter range cells. It is now important to observe the effect of transitions in the clutter power on the design false alarm rate. CFAR detectors are designed to operate in homogeneous independent clutter returns in the training cells. When, for example, an airborne maritime surveillance radar moves from surveying one patch of ocean to another, there may be a change in clutter intensity. This may be due to the presence of a shallow coral reef causing a variation in the sea states in the local area. From a statistical analysis perspective, this phenomenon is studied by slowly varying the clutter power in the CFAR training cells, and estimating the resultant false

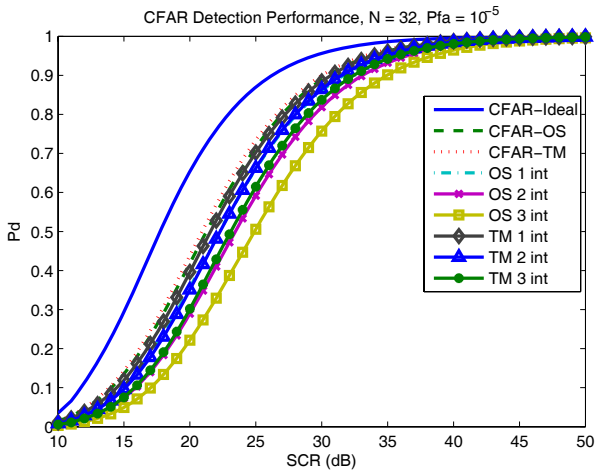

Figure 12: Increasing N to 32 results in further detection improvement, even in the case where there are thee interfering targets. This is for the same scenario as for Figure 11.

alarm probability. Once exactly half of the clutter range cells are completely saturated with higher powered clutter returns, the CUT is then also considered to be infected with higher power clutter. This results in a sharp jump in the estimated probability of false alarm in many cases. Ideally, in a practical CFAR, we would like it to avoid altering the design probability of false alarm. However, it is inevitable during clutter power changes that some variation in the resultant probability of false alarm will occur.

Power will be measured as the mean square of the Pareto distribution. Hence for a Pareto distribution with parameters α and β, the power ρ can be shown to be $\rho = \alpha\beta^2/(\alpha - 2)$. In order to examine clutter transitions, we suppose the scale parameter β remains constant, without loss of generality, while the shape parameter is varied to correspond to a required dB power change. To this end, by applying ρ, if our first Pareto clutter distribution has shape parameter α_1, while the second has α_2, then for an x dB clutter change, it is required that

$$\alpha_2 = \frac{2}{\left(1 - 10^{-0.1x}\left\{\frac{\alpha_1 - 2}{\alpha_1}\right\}\right)}.$$

8.1 Horizontal Polarisation

For the case of horizontal polarisation, the numerical examples are based upon Pareto clutter with parameters $\alpha = 4.7241$ $\beta = 0.0446$, as used previously. In all cases, the number of clutter cells is $N = 16$, so that the OS- and TM-CFARs use the same censoring parameters as before. All estimated false

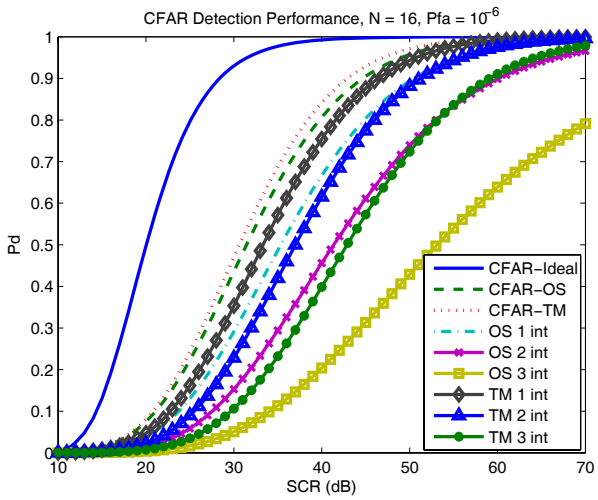

Figure 13: Detector performance, in horizontally polarised clutter, with the probability of false alarm reduced, and the SCR of each interfering target increased to 10 dB.

alarm probabilities have been generated using Monte Carlo estimation, with 10^6 runs in each case. Figure 17 is for a design false alarm probability of 10^{-5}, and the clutter power is slowly increased by 0.5 dB. This is done by gradually increasing the number of higher powered clutter cells. The clutter power increase is referred to as the clutter to clutter ratio (CCR). The Figure shows the effect on the false alarm probability for both the OS- and TM-CFARs. In all cases the logarithm of the estimated probability of false alarm is plotted. The OS-CFAR's resultant probability of false alarm immediately increases, and then remains almost constant at approximately $10^{-0.5}$, which is unacceptably high in practice. The TM-CFAR does not experience such a huge change until its CUT is also infected with higher power clutter. Observe that a 0.5 dB change is a very small power increase, but it is enough to result in false alarm probability increases.

For a second example, Figure 18 shows the effect on the probability of false alarm, when the design one is 10^{-6} and the clutter power is increased by 1 dB. The same phenomenon occurs as for Figure 17, although the TM-CFAR performs better.

Figure 19 shows the performance when the clutter transition is now by 5 dB. The design false alarm probability is still 10^{-6}, and we observe the TM-CFAR does a better job than before, until the point where the CUT is also affected by higher powered returns.

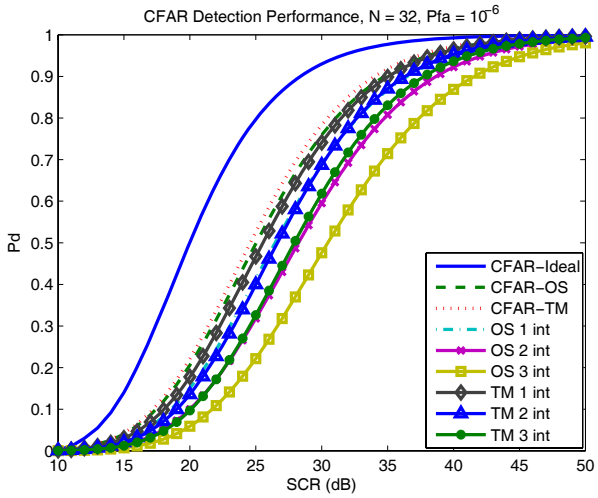

Figure 14: Result of increasing N for the scenario depicted in Figure 13.

8.2 Vertical Polarisation

Some examples of clutter transitions are now provided for the case of vertical polarisation. For the two examples provided, the clutter has been based upon a Pareto distribution with parameters $\alpha = 15.8983$ and $\beta = 0.1812$, as considered previously. Figure 20 shows a typical result, where $N = 16$, and the design false alarm probability is 10^{-5}. The clutter power is increased by a factor of 0.5 dB. What tends to happen with this polarisation is that the TM-CFAR tends to result in a reduction in the probability of false alarm. Once the CUT is affected, the probability of false alarm increases as shown. The OS-CFAR results in the same estimated probability of false alarm behaviour as for the horizontally polarised case.

Figure 21 shows the resultant probability of false alarm when the design probability of false alarm is increased to 10^{-4} and the clutter power is increased by 1 dB. The TM-CFAR results in a reduction in the probability of false alarm as before, before increasing as shown.

In other examples considered, when the probability of false alarm is reduced to less than 10^{-5}, the TM-CFAR yields a sharper drop in the resultant false alarm probability, before jumping to a higher level, as illustrated in Figures 20 and 21.

8.3 Conclusions

All CFAR processes experience a change in their design probability of false alarm when subjected to clutter transitions. The TM-CFAR tended to have more desirable behaviour than the OS-CFAR. Its performance can be improved, however, by increasing the number of lower-censored clutter statistics.

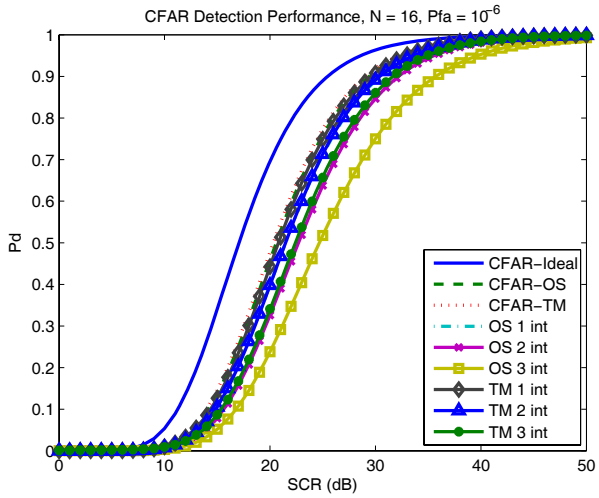

Figure 15: Detector perfromance, with vertically polarised clutter, with up to three interfering targets, each with SCR of 10 dB.

However, this can result in detection losses in homogeneous clutter because of the reduction in the number of clutter range cells.

9 Optimal Detector Considerations

From the examples considered in Section 6, it is clear that in the homogeneous clutter case that there is no single dominant CFAR detector. This is, of course, relative to a Swerling 1 target model, and the same observation was reported in [17]. In the next few Sections this is examined further. To this end, it is worth considering the probability of detection of (5) for a general target model. Note that its detection probability is given by

$$\begin{aligned} \mathbf{Pd} &= \mathbb{P}\left(Z > \beta^{1-N\tau} \prod_{j=1}^{N} X_j^{\tau} \,\middle|\, H_1 \right) \\ &= \mathbb{P}\left(\log\left(\frac{Z}{\beta}\right) > \tau \sum_{j=1}^{N} \log\left(\frac{X_j}{\beta}\right) \,\middle|\, H_1 \right) \\ &= \mathbb{P}\left(\log\left(\frac{Z}{\beta}\right) > \tau W \,\middle|\, H_1 \right), \end{aligned} \tag{18}$$

where W is a Gamma random variable with parameters N and α, as explained in [17]. It is interesting to observe that if the CUT statistic, under H_1, has a Pareto distribution $Pa(\alpha(1+S), \beta)$, for some $S > 0$, then the probability of detection (18) reduces to the Gaussian intensity case, where S is the target

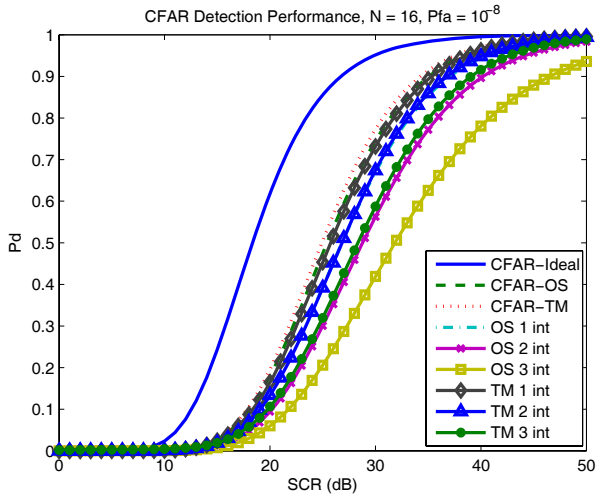

Figure 16: Result of decreasing the probability of false alarm for the scenario in Figure 15.

signal to clutter ratio (see [19]), with an application of (4). As a consequence of this, it follows by the optimality of the cell-averaging CFAR in Gaussian distributed intensity clutter, any CFAR process produced by the approach of [17] with a $Pa(\alpha(1+S),\beta)$ clutter and target model will have smaller detection probability than that of (5). Given the preservation of the UMP property under simple transformations [24], this suggests that (5) is the optimal decision rule, relative to the underlying target model. On the surface, this appears to have answered the question of interest. However, it is important to now consider the properties of the signal yielding the CUT statistic under H_1.

10 Signal Analysis

For the CUT statistic Z to have a $Pa(\alpha(1+S),\beta)$ intensity distribution under H_1, the signal plus clutter in the complex domain must necessarily have a compound Gaussian formulation, with inverse Gamma texture distribution with parameters $\alpha(1+S)$ and β [9]. It is hence important to explore the form of the signal that generates this CUT statistic. The latter arises as an intensity measurement of a single complex signal added to complex clutter.

A random variable D has an inverse Gamma distribution if its density has the form $g_D(t) = \frac{2\beta^{\alpha}}{\Gamma(\alpha)}t^{-2\alpha-1}e^{-\beta t^{-2}}$, for $t \geq 0$, where α and β are non-negative distributional parameters. We write $D \stackrel{d}{=} IG(\alpha,\beta)$. Using the theory of spherically invariant random processes (SIRPs), it can be shown that when this distribution is used for the texture component of a compound Gaussian model, the resultant marginal intensity model is Pareto distributed, with shape

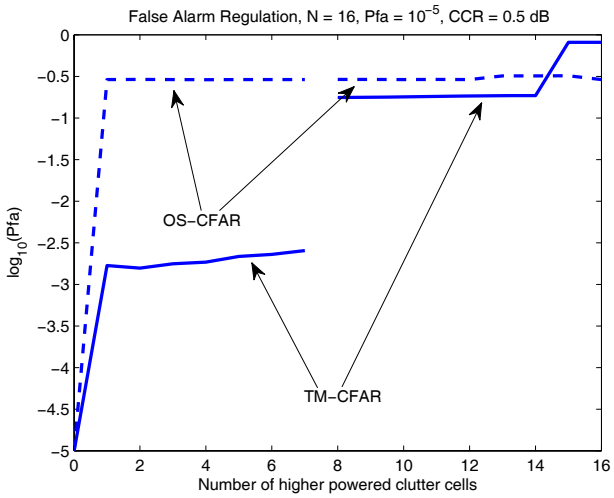

Figure 17: Example of the result of clutter changes on the design probability of false alarm. This example is for the case of horizontal polarisation, and when the clutter power is increased by 0.5 dB. This is done by slowly increasing the clutter power in the CFAR training cells. When the middle point of the range cells is affected by higher powered clutter, the CUT is then also considered infected by the higher power. This explains the sudden jump in the estimated probability of false alarm.

parameter α and scale parameter β [9].

Suppose $\boldsymbol{c}$ is the clutter in the CUT in the complex domain. Then we can express it in the form $\boldsymbol{c} = \omega_1 \boldsymbol{\mathcal{G}}_1$, where $\omega_1 \stackrel{d}{=} IG(\alpha, \beta)$ is the inverse Gamma texture, and $\boldsymbol{\mathcal{G}}_1$ is a bivariate 2×1 zero mean vector Gaussian process with covariance matrix M_1, which is a 2×2 matrix. If the signal in the CUT is $\boldsymbol{s}$, then from the previous analysis, we require $\boldsymbol{s} + \boldsymbol{c} = \omega_2 \boldsymbol{\mathcal{G}}_2$, where $\omega_2 \stackrel{d}{=} IG(\alpha(1+S), \beta)$ and $\boldsymbol{\mathcal{G}}_2$ is a zero mean vector bivariate Gaussian process with 2×2 covariance matrix M_2. It will be assumed, without loss of generality, that $\boldsymbol{s}$ and $\boldsymbol{c}$ are independent processes. Furthermore, it is required that $\boldsymbol{s}$ can be generated without dependence on the Pareto clutter parameters. Although the signal can locally affect the clutter returns, it is assumed here that these two processes are separate.

Reverting to complex forms, we can write $\boldsymbol{s}+\boldsymbol{c} = \|\boldsymbol{s}+\boldsymbol{c}\|e^{i\Theta}$ and $\boldsymbol{c} = \|\boldsymbol{c}\|e^{i\Phi}$, where Θ and Φ are independent phases, assumed to be uniformly distributed on the interval $[0, 2\pi]$, and $\|\cdot\|$ is the complex modulus. Then it follows that

$$\begin{aligned} \boldsymbol{s} &= \|\boldsymbol{s}+\boldsymbol{c}\|e^{i\Theta} - \|\boldsymbol{c}\|e^{i\Phi} \\ &= \begin{bmatrix} \|\boldsymbol{s}+\boldsymbol{c}\|\cos(\Theta) - \|\boldsymbol{c}\|\cos(\Phi) \\ \|\boldsymbol{s}+\boldsymbol{c}\|\sin(\Theta) - \|\boldsymbol{c}\|\sin(\Phi) \end{bmatrix}, \end{aligned} \tag{19}$$

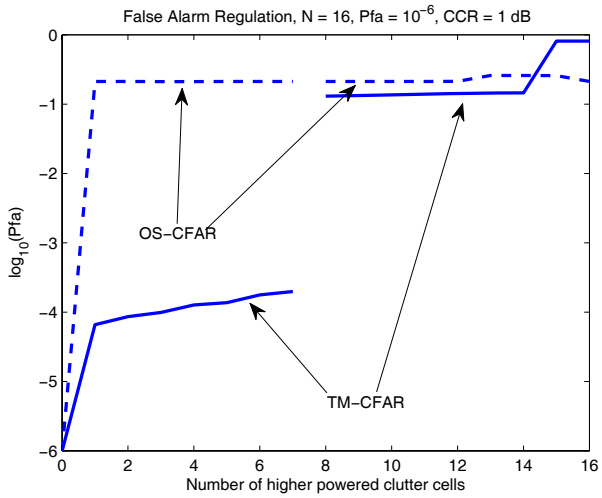

Figure 18: False alarm regulation: same scenario as for Figure 17, except with a 1 dB power increase.

where the 2×1 matrix has elements the real and imaginary components of $\boldsymbol{s}$, and is used for brevity. The signal's intensity is analysed to determine its properties. Taking the modulus of expression (19) shows that

$$\|\boldsymbol{s}\|^2 = \|\boldsymbol{s}+\boldsymbol{c}\|^2 + \|\boldsymbol{c}\|^2 - 2\|\boldsymbol{s}+\boldsymbol{c}\|\|\boldsymbol{c}\|\cos(\Theta - \Phi), \tag{20}$$

using a simple trigonometric identity. Intensity (20) can be further reduced to a function of its underlying random components. To this end, the following Lemma is required:

Lemma 10.1 *If* $Q \stackrel{d}{=} Pa(\alpha, \beta)$ *then* $\sqrt{Q} \stackrel{d}{=} Pa(2\alpha, \sqrt{\beta})$.

The proof of the Lemma follows by directly evaluating the distribution functions.

Applying Lemma 10.1, together with (4), to (20), it follows that the signal intensity can be written

$$\|\boldsymbol{s}\|^2 = \beta\left[e^{Y_1} + e^{Y_2} - 2e^{Y_3+Y_4}\cos(\Phi - \Theta)\right], \tag{21}$$

where $Y_1 \stackrel{d}{=} Exp(\alpha(1+S)), Y_2 \stackrel{d}{=} Exp(\alpha), Y_3 = 0.5Y_1$ and $Y_4 = 0.5Y_2$. It is also not difficult to show that $\cos(\Phi - \Theta)$ is uniformly distributed on the interval [-1, 1].

What is immediate from (21) is that the signal's intensity distribution varies directly with the clutter parameters. This means the signal $\boldsymbol{s}$ cannot be decoupled from $\boldsymbol{c}$, meaning no complex form will yield a CUT statistic under H_1 with the desired Pareto distribution.

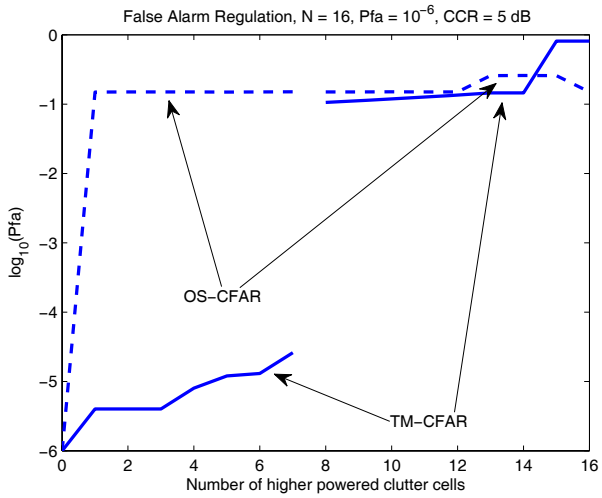

Figure 19: Result of increasing the clutter power change to 5 dB, for the same scenario in Figure 18.

Observe that, by taking expectations in (21), and using the assumed independence of respective random variables, together with the fact that the mean of $\cos(\Phi - \Theta)$ is zero,

$$\mathbb{E}\|\boldsymbol{s}\|^2 = \beta \left[M_{Y_1}(1) + M_{Y_2}(1) \right], \tag{22}$$

where $\mathbb{E}$ is the mean with respect to $\mathbb{P}$ and $M_Y(t)$ is the moment generating function of Y [20]. Since Y_1 and Y_2 are both Exponentially distributed, it can be shown that the mean squared (22) reduces to

$$\mathbb{E}\|\boldsymbol{s}\|^2 = \alpha\beta \left[\frac{(1+S)(2\alpha - 1) + 1}{(\alpha - 1)(\alpha(1+S) + 1)} \right]. \tag{23}$$

The mean of the signal's intensity clearly demonstrates the dependence the process $\boldsymbol{s}$ has on α and β. Figure 22 shows a series of plots of (23), as a function of α, for $S = 10$ dB fixed, and with three values of β.

For an alternative perspective, an example is now included to illustrate the signal's strong dependence on the Pareto clutter parameters directly. Consider the signal's intensity embedded within the two Pareto clutter distributions: $Pa(5, 0.01)$ and $Pa(5.5, 0.05)$. The SCR has been set to $S = 3$ dB, and 1,000 independent realisations have been produced of (21) using simulation. Figure 23 shows the signal embedded within the first clutter set, while Figure 24 is for the second. Figure 25 plots the empirical distribution functions of each of the signals in the respective clutter.

The sample mean for the first signal is 0.2037, with a variance of 0.0422. For the second signal, the sample mean is 1.0999 with variance 1.2310. These figures and results illustrate the strong dependence the signal has on the clutter parameters.

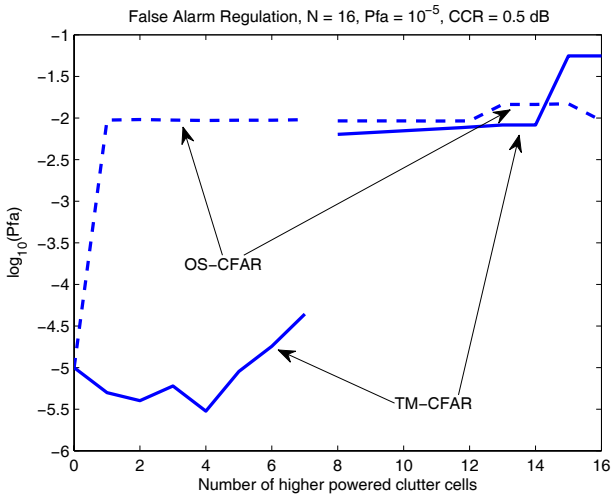

Figure 20: Clutter transitions in vertically polarised clutter, with a 0.5 dB clutter power increase.

11 Conclusions

A series of new CFAR detectors, for target detection in Pareto distributed clutter, were introduced. It was found that, in the case of homogeneous clutter, these new CFARs did not significantly improve on those introduced in [17]. However, in the case where the clutter range cells contained multiple interfering targets, the TM-CFAR, with automatically adjusted trimming points, could be designed to manage a number of such targets. In the context of managing the design false alarm rate, the TM-CFAR did a generally good result, until the CUT became saturated. This detector, however, is more robust for practical CFAR implementation in a real system. It also improved on the performance of the CFARs introduced in [17], in the non-homogeneous clutter case.

The existence of an optimal CFAR detector for Pareto clutter models was also examined in this paper. It is clear that with a Swerling 1 target model, there is no single domainant detector, as in the Gaussian intensity case. It was also shown that it is impossible to produce a signal, independent of the clutter, that results in the dominance of the product CFAR (5).

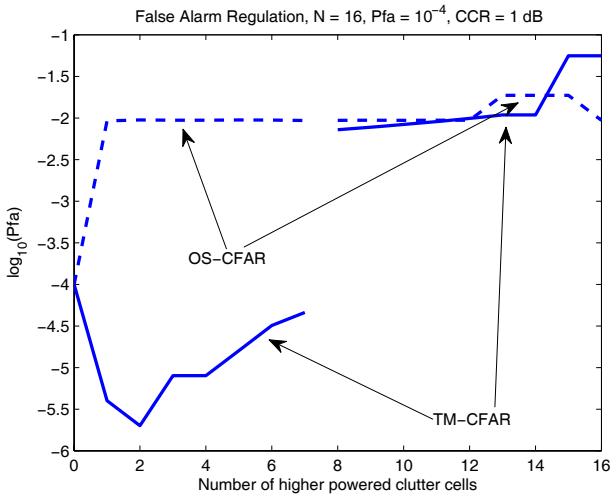

Figure 21: Clutter transitions in the vertically polarised case, for a larger false alarm probability than that used for Figure 20, with a 1 dB clutter increase.

References

[1] D. A. Shnidman, Generalized Radar Clutter Model, IEEE Transactions on Aerospace and Electronic Systems, 35, 1999, 857-865.

[2] J. L. Marcum and P. Swerling, Studies of target detection by pulsed radar, IEEE Transactions on Information Theory, IT-6, 1960, 59-308.

[3] G. V. Trunk and S. F. George, Detection of Targets in Non-Gaussian Sea Clutter, IEEE Transactions on Aerospace and Electronic Systems, AES-6, 1970, 620-628.

[4] D. C. Schleher, Radar Detection in Weibull Clutter, IEEE Transactions on Aerospace and Electronic Systems, AES-12, 1976, 736-743.

[5] E. Jakeman and P. N. Pusey, Statistics of Non-Rayleigh Sea Echo, IEE Radar Conference Proceedings, 155, 1977, 105-109.

[6] K. D. Ward, Compound Representation of High Resolution Sea Clutter, IEE Electronics Letters, 17, 1981, 561-563.

[7] G. V. Weinberg, Coherent Multilook Radar Detection for Targets in KK-Distributed Clutter, in Digital Communication, C. Palanisamy (Ed.), Intech, Croatia, 2012.

[8] A. Balleri, A. Nehorai and J. Wang, Maximum Likelihood Estimation for Compound-Gaussian Clutter with Inverse-Gamma Texture, IEEE Transactions on Aerospace and Electronic Systems, 43, 2007, 775-780.

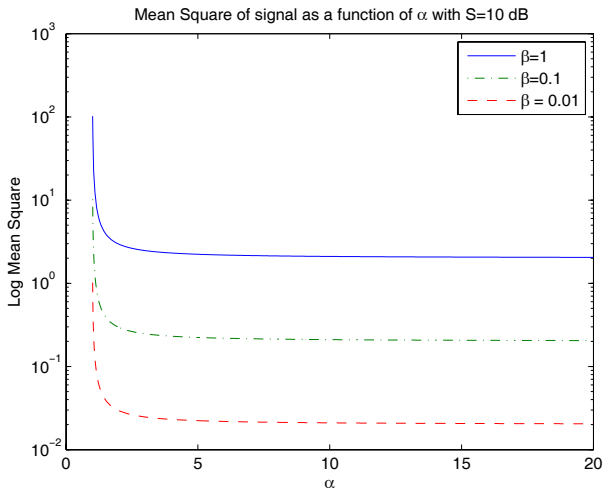

Figure 22: Demonstration that the mean square of the signal varies with the clutter parameters.

[9] G. V. Weinberg, Coherent Multilook Radar Detection for Targets in Pareto Distributed Clutter, IET Electronics Letters, 2011, 47, 822-824.

[10] M. Farshchian and F. L. Posner, The Pareto Distribution for Low Grazing Angle and High Resolution X-Band Sea Clutter, IEEE Radar Conference Proceedings, 2010, 789-793.

[11] G. V. Weinberg, Assessing the Pareto Fit to High Resolution High Grazing Angle Sea Clutter, IET Electronics Letters, 2011, 47, 516-517.

[12] X. Shang and H. Song, Radar detection based on compound-Gaussian model with inverse gamma texture, IET Radar, Sonar and Navigation, 5, 2011, 315-321.

[13] K. J. Sangston, F. Gini and M. S. Greco, Coherent Radar Target Detection in Heavy-Tailed Compound Gaussian Clutter, IEEE Transactions on Aerospace and Electronic Systems, 48, 2012, 64-77.

[14] G. V. Weinberg, Assessing Detector Performance, with Application to Pareto Coherent Multilook Radar Detection, IET Radar, Sonar and Navigation, 2013, 7, 401-412.

[15] G. V. Weinberg, Coherent CFAR Detection in Compound Gaussian Clutter with Inverse Gamma Texture, EURASIP Advances in Signal Processing, 2013, 1.

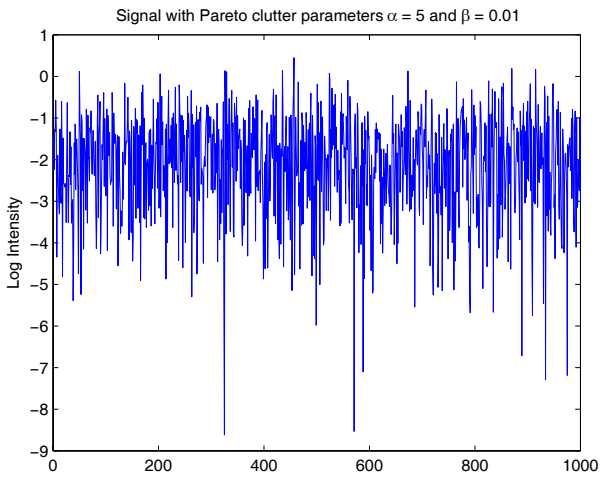

Figure 23: The signal with a $Pa(5, 0.01)$ clutter model, where the logarithm of the signal's intensity is plotted.

[16] G. V. Weinberg, Analysis of Classical Incoherent Integrator Radar Detectors in Compound Gaussian Clutter, IET Electronics Letters, 49, 2013, 213-215.

[17] G. V. Weinberg, Constant False Alarm Rate Detectors for Pareto Clutter Models, IET Radar, Sonar and Navigation, 7, 2013, 153-163.

[18] G. V. Weinberg, Estimation of Pareto clutter parameters using order statistics and linear regression, IET Electronics Letters, 49, 2013, 845 - 846.

[19] P. P. Gandhi and S. A. Kassam, Optimality of the Cell Averaging CFAR Detector, IEEE Transactions on Information Theory, 40, 1994, 1226-1228.

[20] G. P. Beaumont, Intermediate Mathematical Statistics, Chapman and Hall, London, 1980.

[21] M. Evans, N. Hastings and B. Peacock, Statistical Distributions, Wiley, New York, 2000, 3rd Edition.

[22] G. Minkler and J. Minkler, CFAR: The Principles of Automatic Radar Detection in Clutter, Magellan, Baltimore, 1990.

[23] N. Levanon, Radar Principles, John Wiley and Sons, New York, 1988.

[24] A. Ghobadzadeh, A. A. Tadaion and M. Taban, Transformation Effects on Invariant Property of Invariant Hypothesis Test and UMPI detector, Proceedings of the International Symposium on Information Theory, 2009, 977-980.

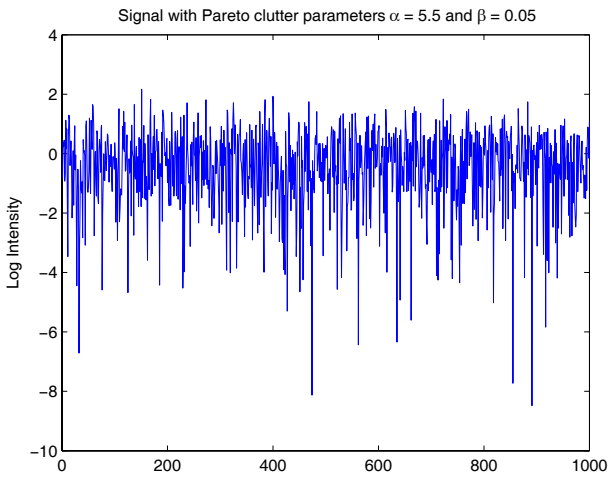

Figure 24: The signal when the clutter follows a $Pa(5.5, 0.05)$ distribution, also plotted as logarithmic intensity.

[25] P. P. Gandhi and S. A. Kassam, Analysis of CFAR Processors in Nonhomogeneous Background, IEEE Transactions on Aerospace and Electronic Systems, 24, 1988, 427-445.

[26] N. J. S. Stacy and M. P. Burgess, Ingara: the Australian Airborne Imaging Radar System, Proceedings of the International Geoscience and Remote Sensing Symposium, 1994, 2240 - 2242.

[27] N. Stacy, D. Crisp, A. Goh, D. Badger and M. Preiss, Polarimetric Analysis of Fine Resolution X-Band Sea Clutter Data, Proceedings of the International Geoscience and Remote Sensing Symposium, 2005, 2787-2790.

[28] M. Greco, F. Gini and M. Rangaswamy, Statistical analysis of measured polarimetric clutter data at different range resolutions', IEE Proceedings -Radar, Sonar and Navigation, 153, 2006, 473-481.

Received: July 1, 2013

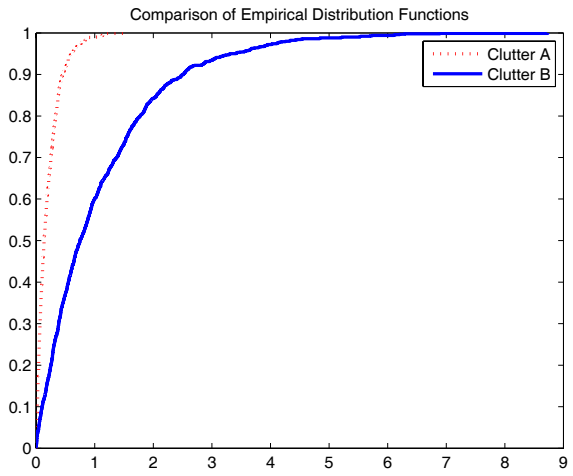

Figure 25: A comparison of empirical distribution functions for each of the two signal cases plotted in Figure 1 and 2. Clutter A refers to the $Pa(5, 0.01)$ model, while Clutter B is for $Pa(5.5, 0.05)$.